A mathematical model for the progression of dental caries

RENE FABREGAS[1,2] AND J. RUBINSTEIN[1]

[1]*Department of Mathematics, Technion-Israel Institute of Technology, Amado Building, Haifa, 32000, Israel.*

[2]*Department of Applied Mathematics, Complutense University, Séneca 2 Street, Madrid, 28040, Spain.*

A model for the progression of dental caries is derived. The analysis starts at the microscopic reaction and diffusion process. The local equations are averaged to derive a set of macroscopic equations. The global system includes features such as anisotropic diffusion and local changes in the geometry due to the enamel melting. The equations are then solved numerically. The simulations highlight the effect of anisotropy. In addition we draw conclusions on the progression rate of caries, and discuss them in light of a number of experiments.

Keywords: Dental Caries, Mathematical Modeling, Numerical Simulation, Caries Progression Rate.

1. Introduction

Dental caries is the process where the mineral components of the tooth dissolve and break down. The underlying process starts with bacteria in the mouth that digest foodstuff such a sucrose, and convert them into acidic material such as lactic acid. Hydrogen ions that dissolve from the lactic acid penetrate into the tooth and react with its mineral compounds such as enamel or dentin. As the enamel dissolves, the tooth become mechanically weak and susceptible to local collapse, which leads to the formation of cavities.

Our goal is to derive a mathematical model for the first part of this process, namely the dissolution of the enamel. The model starts from the local transport equations on the microscopic scale. The local equations are averaged via the method of homogenization to create a macroscopic model. Our model takes into account key factors such as the anisotropic geometry of the enamel and the time evolution of the microstructure due to demineralization and remineralization.

The outer layer of the tooth is formed of enamel. This is a mineral consisting of a packed array of rods, called sometimes enamel prisms. A rod's length is about 8 microns, and its radius is about 1 micron. In healthy enamel the rods are separated by a distance under 1 micron. Each rod consists of hydroxyapatite crystals. Enamel is created in the human body at infanthood. It is not generated later in life. However, even upon demineralization through caries, the process is reversible, and remineralization can take place.

In the tooth the rods are arranged roughly in layers, where the long axis is perpendicular to the tooth surface. The inter-rod domain consists of pores and of material that has the same chemical composition as enamel, but the crystal orientation is not ordered as in the rods themselves. It is known that diffusion in the enamel is mostly along the prisms (rods).

Dentin is the material just below the enamel. It is not as hard as enamel, but also not completely different from it. Dentin consists of 70 percent hydroxyapatite crystals, 20 percent organic material, and water. The mineral part of the dentin is not organized in rods as in enamel. However, dentin also has a microscopic structure. It has many tiny channels, dentinal tubules, containing fluid that extend from the

exterior part of it (the enamel-dentin border) to the inner part of the tooth (pulp).

Caries is the process by which enamel is destructed. This process starts when sugar consumed by the person (or animal) is digested by certain oral bacteria. The bacteria form a biofilm on the tooth surface. Since the teeth are naturally abrased, for instance by tooth brushing, these biofilms typically are created in protected areas such as pits and grooves on the tooth surface or near the junction of the tooth and the gums. The common terminology in the literature is to call the area near the pit *occlusal surface*, while the area at the lower part of the tooth is sometimes termed *approximal surface*. The biofilm is typically quite small and concentrated near the pit, while it is spread when it forms at an approximal surface.

The bacteria convert the sugar into lactic acid. This acid reduces the pH level, that is, increases the concentration of hydrogen ions, near the tooth. The ions diffuse into the tooth, thus creating a high acidity environment inside the tooth. This leads to a reaction of the solid (mineral) enamel according to

$$\underset{\text{Hydroxyapatite}}{Ca_{10}(PO_4)_6(OH)_{2(s)}} + 8H_{(aq)}{}^{+} \underset{k_{-1}}{\overset{k_1}{\rightleftharpoons}} 10\,Ca_{(aq)}{}^{2+} + 6\,HPO_4{}^{2-}{}_{(aq)} + 2\,H_2O_{(l)} \tag{1.1}$$

This reaction is reversible, but when the pH level drops to about 5.5 and lower it proceeds mostly to the right. As the enamel is reacting and is demineralized, material is lost and later cavities form in the enamel.

As the enamel dissolves, visible lesions can be observed. We shall focus here on the formation of such lesions where mineral is lost and the porosity increases. We do not consider here the formation of cavities, which is a total mechanical breakdown that occurs after too much mineral is lost.

The propagation of lesions was studied in the last two decades by a number of techniques. We draw particular attention to the work of Bjorndal and his colleagues Bjorland & Thylstrup (1995), Bjorland (2008). The shape of the propagating lesion was summarized by Kidd and Fejerskov Kidd & Fejerskov (2004). When the lesion starts at an approximal surface it has a triangular shape in the enamel, with a base at the enamel surface, and a vertex at the enamel-dentin (ED) junction. Another 'triangle' is then observed at the dentin, with a base at the ED junction and a vertex deep in the dentin. On the other hand, when the lesion starts from a biofilm at a pit at the central top part of the tooth, it has the shape of a triangle with a vertex at the pit (enamel surface) and a base at the ED junction.

An interesting observation of the propagation of enamel lesions and later on of dentin lesions is provided in Bjorland & Thylstrup (1995). Some earlier theories claim that the triangle base at the ED junction forms after the lesion's tip reached the junction, and it is caused by a lateral spread of the lesion at the junction. However, Bjorndal et al. point out that the extent of the triangle base at the ED junction is comparable to the extent of the biofilm (triangular base of the lesion) at the enamel surface. From this, and from other observations they conclude that the lesion base at the dentin starts *before* the lesion reached the junction at the enamel. Rather, they speculate that this base at the ED junction is caused directly by the biofilm. This observation has important clinical implications, as it implies that removing the biofilm can arrest the lesion development.

We also point out this and other papers by Bjorndal and his colleagues, according to which the bacteria hardly spreads into the tooth before cavities are formed. Notice in particular reference Bjorland (2008) for clinical significance of this theory.

In the next section we shall write down the microscopic equations. These equations will be homogenized in section 3, where we take into account the evolution of the microgeometry in space and time. The macroscopic equations involve averaged diffusion coefficients. These coefficients are determined by solving certain canonical differential equations. In section 4 we consider these equations and also discuss the difficult task of estimating the effective diffusivities in a varying local geometry. In section 5

we derive an evolution equation for the microstructure. A number of numerical examples are presented in section 6. Our model and suggestions for extending it are discussed in section 7. Finally, we derive in an appendix a few geometrical identities that we need for the homogenization calculations.

There is a long history of mathematical models for the initial stages of dental caries. For example, we refer to the work of Zimmerman (1966) and Patel *et al.* (1987). These models and others differ in the level of complexity (e.g. the number of compounds) and details of the reaction. They are one-dimensional and thus the anisotropy plays no role. Also, they are written down from the start on a macroscopic level. We start from the microscopic geometry, with the goal of deriving the macroscopic equations. In this process we highlight the importance of the anisotropy of the local enamel geometry, that implies anisotropic diffusion matrix for the different compounds. On the other hand, we shall replace the reaction term (1.1) with a simpler model:

$$\underset{\text{Hydroxyapatite}}{Ca_{10}(PO_4)_6(OH)_{2(s)}} + 8H_{(aq)}{}^{+} \underset{k_{-1}}{\overset{k_1}{\rightleftharpoons}} EMP \tag{1.2}$$

where we use the notation EMP (enamel matrix products) to denote collectively the right hand side of equation (1.1). It is a simple matter to extend our model to account separately for the reaction and diffusion for each of the components of EMP.

2. Local model

We describe a simple model that incorporates some of the basic mechanisms outlined above. The model is only for the formation of the lesion and not formation of cavities. Moreover, in this paper we consider only lesion formation in enamel.

We assume that the biofilm generates hydrogen ions at a given rate. A typical time scale for this is an hour or two following food consumption, since the secretion of the acid takes place after meals.

We consider the enamel to occupy half space $(x_3 > 0, -\infty < x_1, x_2 < \infty)$. The line $x_3 = 0$ is the tooth edge. We assume that the biofilm, i.e. source of acid, occupies a smaller domain $x_3 = 0, -\delta < x_1, x_2 < \delta$. The concentration of H^+ ions is denoted by $H(x,t)$, where $x = (x_1, x_2, x_3)$. There are several processes taking place in the tooth. One is the diffusion and reaction of H^+ ions. A second is diffusion and reaction of the various compounds on the right hand side of equation (1.1). For simplicity we consider here only one such representative compound, denoted by EMP in equation (1.2), and denote its concentration by $c(x,t)$. The description above of the enamel surface and the underlying reactions implies that the diffusion process is macroscopically anisotropic. In fact, we expect caries to be controlled by two general principles. One is that the diffusion coefficients depend on the porosity of the solid, and this, in turn is affected by the enamel density. The second is that diffusion is faster *along* the rods than *across* them. To make the paper easier to read we describe in detail the diffusion and reaction of c, and then homogenize the equation for it. The equation for H can be analyzed and averaged in a similar manner.

The local length scale for the underlying process will be denoted by us l. Because of the size of the enamel prisms and the typical distance between them we set $l = 1\ \mu$. To obtain proper nondimensional variables it is useful to write an ad-hoc one dimensional model (Patel *et al.* (1987), Patel & Fox *et al.* (1987), Bollet-Quivogne & Anderson *et al.* (2005)) consisting of a single reaction diffusion system:

$$c_t = d c_{x_3 x_3} + R(c_s - c). \tag{2.1}$$

Here d is a diffusion coefficient and R is a reaction rate. The parameter c_s is the equilibrium value of the reaction, determined by the acidity, i.e. H, at any given point.

There is a great diversity of estimates for d and R in the literature. We choose here parameters following mostly the papers Bollet-Quivogne & Anderson *et al.* (2005) and Van Duk & Borggreven *et al.* (1983). We thus set $d = 10^4\ \mu^2/h$, $R = 10^{-2}\ 1/h$, and $c_s = 2\cdot 10^{-3}\ g/cm^3$, which corresponds to acidity of about pH =4 Bollet-Quivogne & Anderson *et al.* (2005).

The values of d and R define naturally a length scale

$$\lambda \sim \sqrt{(d/R)} = 100\,\mu. \tag{2.2}$$

This is the length scale where the diffusion and reaction are balanced. For example, consider equation (2.1) in the semi infinite interval $x_3 > 0$, with initial conditions $c(x_3,0) = c_s$. We assume that c approaches c_s for large values of as x_3. Assume further that the boundary condition at $x_3 = 0$ is $c = c_s$, except for bursts of larger $c(0,t)$ of short duration, resulting from a reduction in pH following a meal. In these short bursts a reaction takes place according to equation (2.1). The penetration length of the acidity is thus λ

We point out, though, that the diffusion coefficient d is not fixed in time, since the melting of the enamel increases the size of the pores, and thus increases d. Another point that should be taken into account is that the reaction term (the second term on the right hand side of equation (2.1)) depends not just on c but rather on the difference $c_s - c$. When comparing the reaction term with the diffusion term we assumed that the difference $c_s - c$ is of the same order as c itself. However, when c is near c_s, the reaction term is practically smaller, and then the transition layer is longer. Finally we recall that c_s is determined by the acidity as will be written explicitly below. We thus need to solve for both c and H.

3. Homogenization of the microscopic equations

We assume that the enamel portion of the tooth consists of a volume E occupied by the rods and an inter-rod volume that we denote by V. The ions and enamel matrix solute diffuse in the inter-rod domain V, and might react when they reach the rod boundaries ∂E. We therefore write a diffusion equation for the concentration $c(x_1,x_2,x_3,t)$ in V and appropriate flux condition at the interface ∂E. Since the enamel melts under the reaction with the H^+ ions, we must take into account the time variation of $\partial E(t)$. We thus write the following equations for the diffusion of c and the reaction on ∂E:

$$c_t = D\Delta c, \quad x \in V, \tag{3.1}$$

$$D\partial_n c = R_0(c_s - c) - \bar{v}_n c, \quad x \in \partial E. \tag{3.2}$$

We use here $\bar{v}_n$ to denote the normal velocity of the rod boundary ∂E. We scale the length by λ: $x' = x/\lambda$, and time by $1/R$: $t' = Rt$. In what follows we shall omit the primes to simplify the notation.

Before writing down the scaled equations we describe our model for the microstructure geometry. As noted above the local scale of the prism, which we denoted by l, is much smaller than λ. We thus define the small parameter $\varepsilon = l/\lambda$. We assume that E consists of many elongated prisms (rods) whose thickness is of $O(l)$. The prisms main axis and also their cross section shape varies slowly on the λ - scale. To distinguish between the two length scales we introduce local variables $y_1 = x_1/\varepsilon$, $y_2 = x_2/\varepsilon$. Because of the layered form of the prisms we assume that the geometry is essentially periodic in the y_1, y_2 variables. However we do allow for geometry variations also on the global (x_1,x_2,x_3) scale since different parts of the enamel react at different rates, determined by variations in c.

We denote the inter-rod domain in a single cell by Ω and the enamel cross section in a single cell is denoted by E_p. See Figure 1 for a sketch of simple two cases of a cells containing 1 prism (Figure 1(a)),

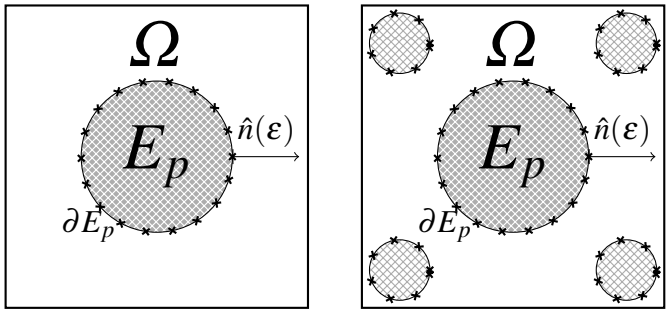

(a) (b)

Figure 1. Examples for the periodic cell cross sections: (a) Local periodic cell containing one prism, (b) Local periodic cell containing 5 prisms.

and 5 prisms (Figure 1(b)) with circular cross sections. It is useful to express the assumptions above on the separation of scales by writing the boundary ∂E_p of the enamel surface via an implicit function

$$\partial E_p : \{(x_1,x_2,x_3,y_1,y_2,t) |\, F(x_1,x_2,x_3,y_1,y_2,t) = 0\}. \tag{3.3}$$

We also need an expression for the normal vector $\hat{n}(\varepsilon)$ to ∂E_p in terms of F. In fact, we need in the sequel only the first two terms in the ε expansion of $\hat{n}$. A straightforward calculation (see the Appendix) gives

$$\hat{n}(\varepsilon) = \hat{\nu} + \varepsilon \left((\hat{\tau} \cdot \nabla_2^x F)/G_F \; \hat{\tau} + \hat{k} F_{x_3}/G_F \right), \tag{3.4}$$

where we introduced the notation $\hat{\nu}$ for the two-dimensional normal to ∂E_p, i.e.

$$\hat{\nu} = \nabla_2^y F/G_F, \quad G_F = |\nabla_2^y F|. \tag{3.5}$$

Here $\hat{\tau}$ denotes the unit two-dimensional tangent vector to ∂E_p, and $\hat{k}$ is a unit vector in the x_3 direction. Also, here and in what follows we use ∇_2^y and Δ_2^y to denote the gradient and Laplacian operators in the two dimensional space (y_1,y_2). Similarly, we use ∇_2^x and Δ_2^x to denote the gradient and Laplacian operators in the two dimensional space (x_1,x_2).

The motion of the boundary of the prism ∂E_p varies on the l local scale. Therefore we write

$$\bar{v}_n = Rl v_n, \tag{3.6}$$

so that v_n is the nondimensional boundary normal velocity. To complete the scaling we normalize the concentration c by a representative value $\bar{c}$ of the equilibrium value c_s, i.e. $c' = c/\bar{c}$.

We are now at a position to write the nondimensional version of equations (3.1)-(3.2):

$$c_t = \Delta c, \quad x \in V, \tag{3.7}$$

$$\partial_n c = \lambda R_0/D(c_s - c) - Rl\lambda/D v_n c, \quad x \in \partial E. \tag{3.8}$$

Because of the elongated shape of the rods, where the long axis extends essentially in the x_3 direction, we expect the solution to vary rapidly in the x_1,x_2 variables. Following the convention in homogenization theory, we thus seek a solution of the from $c(x_1,x_2,x_3,y_1,y_2,t)$. We assume that to leading order $c_s = c_s(x_1,x_2,x_3,t)$. Later on we shall justify this assumption. Since on the present length

and time scales we expect an averaged equation with balanced diffusion and reaction, we also make the assumption that $\lambda R_0/D = \varepsilon R_1$, with $R_1 = O(1)$. Therefore, the boundary condition (3.8) becomes

$$\partial_\nu c = \varepsilon \left(R_1(c_s - c) - v_\nu c - c_{x_3} F_{x_3}/G_F - (\hat{\tau}\cdot\nabla_2^x F)/G_F \; \hat{\tau}\cdot(\nabla_2^x c + 1/\varepsilon \; \nabla_2^y c)\right), \tag{3.9}$$

where v_ν is the two-dimensional velocity of the boundary. We use everywhere ∂_ν to denote the normal derivative in the (x_1,x_2) plane, and ∂_n to denote the normal derivative in the (x_1,x_2,x_3) space.

To solve for c we expand

$$c(x_1,x_2,x_3,y_1,y_2,t) = c^0 + \varepsilon c^1 + \varepsilon^2 c^2 + \ldots \;, c^i = c^i(x_1,x_2,x_3,y_1,y_2,t). \tag{3.10}$$

Upon substituting the expansion into equation (3.7) and the boundary condition (3.9), we obtain a cascade of equations at different orders of ε. At the leading order we obtain

$$\Delta_2^y c^0 = 0, \quad y \in \Omega, \tag{3.11}$$

$$\hat{\nu}\cdot\nabla_2^y c^0 = 0, \quad y \in \partial E_p. \tag{3.12}$$

It is easy to verify that equations (3.11)-(3.12) imply that c^0 is independent of the local scale y, i.e. $c^0 = c^0(x_1,x_2,x_3,t)$.

At the next order we obtain the following equations for c^1:

$$\Delta_2^y c^1 = 0, \quad y \in \Omega, \tag{3.13}$$

$$\hat{\nu}\cdot\nabla_2^y c^1 = -\hat{\nu}\cdot\nabla_2^x c^0, \quad y \in \partial E_p. \tag{3.14}$$

We thus express c^1 in the form

$$c^1(x_1,x_2,x_3,y_1,y_2,t) = W^1(x_1,x_2,x_3,y_1,y_2,t)c^0_{x_1} + W^2(x_1,x_2,x_3,y_1,y_2,t)c^0_{x_2}. \tag{3.15}$$

The *cell functions* W^i solve a *cell problem* of the form

$$\Delta_2^y W^i = 0, \quad y \in \Omega, \tag{3.16}$$

$$\hat{\nu}\cdot\nabla_2^y W^i = -\hat{\nu}_i, \quad y \in \partial E_p. \tag{3.17}$$

Notice that the cell problems are implicitly parameterized by (x_1,x_2,x_3,t) since ∂E_p depends on these variables.

Proceeding to the next level in the expansion we find

$$c^0_t = c^0_{x_3x_3} + \Delta_2^x c^0 + \Delta_2^y c^2 + \nabla_2^y\nabla_2^x c^1 + \nabla_2^x\nabla_2^y c^1, \quad y \in \Omega, \tag{3.18}$$

$$\begin{aligned}\nu\cdot\nabla_2^y c^2 = &-\hat{\nu}\cdot\nabla_2^x c^1 + R_1(c_s - c^0) - v_\nu c^0 - c^0_{x_3}F_{x_3}/G_F - \\ &(\hat{\tau}\cdot\nabla_2^x F)/G_F \; \hat{\tau}\cdot\left(\nabla_2^x c^0 + \nabla_2^y c^1\right), \quad y \in \partial E_p.\end{aligned} \tag{3.19}$$

We integrate equation (3.18) over the cell Ω, and write

$$|\Omega| c^0_t = \int_\Omega \nabla_2^x\cdot(\nabla_2^y c^1 + \nabla_2^x c^0)\, dy + \int_\Omega \nabla_2^y\cdot(\nabla_2^y c^2 + \nabla_2^x c^1)\, dy = J_1 + J_2. \tag{3.20}$$

The integral J_2 on the right hand side is transformed into a boundary term, where we use the boundary condition (3.19), and the fact that c^0 does not depend upon y:

$$J_2 = |\partial E_p| R_1(c_s - c^0) - \left(\int_{\partial E_p} v_\nu\right) c^0 - \left(\int_{\partial E_p} F_{x_3}/G_F\right) c^0_{x_3} - \int_{\partial E_p} (\hat{\tau}\cdot\nabla_2^x F)/G_F \; \hat{\tau}\cdot(\nabla_2^x c^0 + \nabla_2^y c^1). \tag{3.21}$$

To compute the first integral J_1 in equation (3.20) we use the following formula that we prove in the Appendix

$$J_1 = \nabla_2^x \cdot \int_\Omega (\nabla_2^y c^1 + \nabla_2^x c^0)\, dy + \int_{\partial E_p} \nabla_2^x F/G_F \cdot (\nabla_2^y c^1 + \nabla_2^x c^0)\, dy. \tag{3.22}$$

The normal ($\hat{v}$) component of $(\nabla_2^y c^1 + \nabla_2^x c^0)$ vanishes on ∂E_p in light of equation (3.14). The tangential component of this term integrated in the second term on the right hand side of equation (3.22) cancels with the last term on the right hand side of equation (3.21). Next we define the 2×2 matrix

$$\bar{D}_{ij} = \int_\Omega W^i_{y_j}\, dy. \tag{3.23}$$

The computations of J_1 and J_2 and the definition (3.23) enable us to rewrite equation (3.20) in the form

$$|\Omega| c^0_t = |\Omega| c^0_{x_3 x_3} + \sum_{i=1}^{2} \partial_{x_i} \left(\bar{D}_{ij} \partial_{x_j}\right) c^0 + |\partial E_p| R_1 (c_s - c^0) - \left(\int_{\partial E_p} v_\nu\right) c^0 - \left(\int_{\partial E_p} F_{x_3}/G_F\right) c^0_{x_3}. \tag{3.24}$$

Equation (3.24) is the averaged (homogenized) equation for the evolution of c^0. To simplify it, and to recognize it as a conservation law, we make use of two geometric identities that are proved in the Appendix:

$$\int_{\partial E_p} v_n = |\Omega|_t, \quad \int_{\partial E_p} F_{x_3}/G_F = -|\Omega|_{x_3}. \tag{3.25}$$

We now apply identities (3.25) to rewrite equation (3.24) in the form

$$\left(|\Omega| c^0\right)_t = \left(|\Omega| c^0_{x_3}\right)_{x_3} + \sum_{i=1}^{2} \partial_{x_i} \left(\bar{D}_{ij} \partial_{x_j}\right) c^0 + |\partial E_p| R_1 (c_s - c^0). \tag{3.26}$$

Notice that we wrote the derivatives of c^0 with respect to x_3 and with respect to (x_1, x_2) separately to emphasize the symmetry breaking induced by the prism geometry.

Equation (3.26) is not closed, since the enamel E_p melts and therefore both $|\partial E_p|$ and $|\Omega|$ change in time and space. In addition, the effective diffusion tensor $\bar{D}$ depends upon the concentration c^0. This issue will be addressed in the next section. We still need to determine the solubility term c_s. From the simplified reaction equation (1.2) we have $c_t = k_1 XH - k_2 c$, where we denote by X the hydroxyapatite concentration. Therefore the term c_s is proportional to the concentration H of the hydrogen ions, and we write explicitly $c_s = \gamma H$. Our estimate in the preceding section for c_s at pH=4 implies $\gamma \sim 40$.

We need also to evaluate the macroscopic equation for H. However, the hydrogen ions diffuse and react in the same geometry as the EMP. Therefore the same homogenization procedure that was performed in this section applies also to H. There are two differences, though. First, the hydrogen ions are much smaller than the EMP molecules, and therefore its diffusion coefficient is quite larger. Thus we assume that on the time scale on which c evolves, the distribution of H is at equilibrium. Still H depends on time implicitly through the boundary conditions on the tooth surface, as will be explained in more detail via examples below. Secondly, the amount of ions lost to the reaction is small compared to the total amount of ions, and therefore we can neglect the reaction term. Thus, the equation for H is

$$\left(|\Omega| H_{x_3}\right)_{x_3} + \sum_{i=1}^{2} \partial_{x_i} \left(\bar{D}_{ij} \partial_{x_j}\right) H = 0. \tag{3.27}$$

We also write the final equation for the evolution of the EMP in the form

$$(|\Omega|c)_t = \left(|\Omega|c_{x_3}\right)_{x_3} + \sum_{i=1}^{2} \partial_{x_i}\left(\bar{D}_{ij}\partial_{x_j}\right)c + |\partial E_p| R_1(\gamma H - c), \tag{3.28}$$

where we omitted the 0 superscript for convenience. In section 6 we shall address the question of initial and boundary conditions for these two equations.

4. The cell problem for the effective diffusion coefficients

To solve the homogenized equations (3.27) - (3.28) we need to compute the effective diffusion matrix $\bar{D}$. This requires solving the cell problem (3.16)-(3.17). Moreover, since the shape of the enamel E_p evolves in space and time, we need to solve the cell problem for each time iteration and at all space points (on the x scale). To simplify this task, and since the local prim changes slowly in space on its local y scale, we assume that the enamel motion is averaged, in the sense that the boundary ∂E_p moves normal to itself, and therefore the shape E_p forms a one-dimensional family of domains. The matrix $\bar{D}$ can be computed for a number of representative shapes from this family, and then the value of $\bar{D}$ for an actual shape can be determined by interpolation from the computed family.

For example, we demonstrate this idea for the simple case where the cell consists of the 2×2 square, and E_p is a disc of radius ρ at its center, as depicted in Figure 1(a). Symmetry implies that in this case $\bar{D}$ is of the form $\bar{D} = dI$ where $d(\rho)$ is an effective diffusion coefficient, and I is the 2×2 identity matrix. Solving the cell problem for this geometry gives the curve $d(\rho)$ as depicted in the dotted line in Figure 2(a).

5. Enamel dissolution

In this section we couple the effective reaction diffusion equation to the enamel dissolution process. The diffusion and reaction are described by equation (3.28). Recall that we used the length λ as a length unit and $1/R$ as a time unit. Also, the cell area $|\Omega|$ and the prism boundary $|\partial E_p|$ are computed on the local y scale (l), and therefore they are both $O(1)$ objects.

To verify that the model is consistent, and to estimate the parameter R_1, we give a rough estimate of the enamel dissolution. We thus concentrate on the global reaction term

$$(|\Omega|c)_t \sim R_1|\partial E_p|(c_s - c). \tag{5.1}$$

We return to dimensional units, using 1h for the time variable and 1μ for the length variable. In light of the enamel basic symmetry we concentrate on a two dimensional slice of the enamel. The concentration c is expressed in units of mol/μ^2. Indeed the relation (5.1) is convenient for use in computing reaction terms since it expresses the chemical quantities in units of moles. The reaction model (1.2) relates the number of hydroxyapatite molecules to the number of EMP molecules. Denote the number of c molecules in Ω (per 1cm in the x_3 coordinate) by N^c, and similarly the number of hydroxyapatite molecules in E_p (per 1cm in the x_3 direction) is denoted N^e. We thus write

$$N_t^e = -N_t^c. \tag{5.2}$$

The reaction relation (5.1) can be written as

$$N_t^e \sim -R_1|\partial E_p|(c_s - c). \tag{5.3}$$

To convert this result to the rate of change of E_p itself we need to compute the molar concentration of hydroxyapatite. This can be computed from the known value of the molar mass of this molecule (500 g/mol) and its known density (3000 g/Liter). Thus the molar concentration of enamel is

$$\kappa^e = 6 \text{ mol/Liter} = 6 \cdot 10^{-11} \frac{\text{mol}}{\mu^2\, cm}. \tag{5.4}$$

Using the formula $\kappa^e = N^e/|E_p|$, and since κ^e is constant in time, we obtain

$$|E_p|_t = -\frac{|\partial E_p| R_1}{6} 10^{11} (c_s - c). \tag{5.5}$$

For example, we assume that a cell is of size 2×2, and the prism radius is 1. Thus there are approximately $0.25 \cdot 10^8$ prisms in a 1 cm^2 square. Assume further an acidity of pH=4, which corresponds to $c_s \sim 10^{-14}\text{mol}/\mu^2$. Then, denoting the total enamel volume (per 1 cm in the x_3 direction) by $\tilde{E}$, we obtain $\tilde{E}_t \sim -2.5 R_1 \cdot 10^{-4}$ cm^2/h. Recalling that the mass density of the enamel is about 3 g/cm^2, we obtain that the rate of mass loss per unit area is

$$m_t \sim 7.5 R_1 10^{-4} \text{g/h cm}^2. \tag{5.6}$$

This compares favorably, using an $O(1)$ value for R_1, with experimental data Holly & Gray (1968), Anderson *et al.* (1998).

To complete the unknown parameters and functions in equation (3.27) we need to obtain an equation for the volume $|\Omega|$, the surface area ∂E_p, and the effective tensor $\bar{D}$. Our starting point is equation (5.5) which we write slightly differently as

$$|E_p|_t = -|\partial E_p| \frac{R_1}{\kappa} (c_s - c). \tag{5.7}$$

A precise melting equation requires an evolution equation not just for the area $|E_p|$ but also for the prisms shape. In general this involves a complex moving boundary problem. However, since the concentration c varies slowly on the scale of individual prisms we propose a simplified model, as explained in the previous section. For example, we assume that initially E_p is a disc, and this shape does not change appreciably as the prism melts. Thus the function $E_p(x,t)$ is characterized by a single parameter, namely the radius $\rho(x,t)$ of the prism. Therefore, we can express both the surface area $|\partial E_p|$ and the area $|\Omega|$ using ρ. The evolution of ρ is easily obtained form equation (5.7). Denoting the cell, including the prism, by $\bar{\Omega}$, we write $|\Omega| = |\bar{\Omega}| - \pi\rho^2$, $|\partial E_p| = 2\pi\rho$. It follows that ρ evolves according to

$$\rho_t = -\frac{R_1}{\kappa} (c_s - c) = \frac{R_1}{6} (c_s - c), \tag{5.8}$$

where in the last term we express the concentrations c_s and c in units of mol/Liter. Similarly, we can construct a more complex local prism geometry, such as a collection of discs of different radii at every cell, where each of the discs evolves by equation (5.8).

We now summarize the nonlinear diffusion-dissolution system that we derived: The concentration c of the enamel matrix products is determined by equation (3.28). It is practically convenient to scale c by γ and write $c = \gamma q$, The scaled EMP concentration q satisfies the equation

$$(|\Omega| q)_t = \left(|\Omega| q_{x_3}\right)_{x_3} + \sum_{i=1}^{2} \partial_{x_i} \left(\bar{D}_{ij} \partial_{x_j}\right) q + |\partial E_p| R_1 (H - q), \tag{5.9}$$

The area $|\Omega|$ and surface area $|\partial E_p|$ are computed using equation (5.8) for the local radius $\rho(x,t)$. for future reference we rewrite this equation in a scaled form:

$$\rho_t = -\frac{R_1}{6}\gamma(H-q)\,. \tag{5.10}$$

The ion concentration H is in a quasi steady state, determined by equation (3.27). Finally, The diffusion tensor $\bar{D}$ is computed from equations (3.16)-(3.17) and the integral (3.23).

6. Numerical examples

In this section we consider the numerical implementation of the model derived in the previous sections. We also give numerical examples.

The evolution equations for c (or q) and H are solved in a finite domain. Also, for simplicity we restrict the examples to two spatial dimensions. The anisotropy of the diffusion process is already manifested in this case. We thus consider in all the examples below the domain to be

$$V = \{-1 < x_1 < 1,\ \ 0 < x_3 < 3\}.$$

This domain is similar to samples used in a number of experiments.

The diffusion equation (5.9) can be handled by standard methods for parabolic equations, such as Crank-Nicolson or ADI. One special feature is that we need to update at each time step the geometric functions $|\Omega(x,t)|$ and $|\partial E_p(x,t)|$. As explained above, this can be done by updating at each time step the radius function $\rho(x,t)$. A second, more difficult point, is the computation of the effective diffusion tensor $\bar{D}$. Since the local cell geometry varies as a function of x and t, we must solve the cell problem (3.16)-(3.17) and then compute the integral (3.23) for each local value of $\rho(x,t)$. For instance, when solving the equations numerically, we need to find this tensor at each grid point (in space and time). This is a hard problem even under the simplification that E_p is characterized by a single disc. We thus propose a method to overcome this problem. The idea is to compute *apriori* the tensor $\bar{D}$ as a function of the radius ρ for a finite set of values $(\rho_1, \rho_2, .., \rho_n)$. Then, at each point (x,t) we interpolate $\bar{D}(\rho(x,t))$ from the precomputed set of $\bar{D}$.

We examined several interpolation models. For example, consider the case where each cell has a single disc. In Figure 2(a) we compare the exact $\bar{D}$ for this case to a linear interpolation of it, and in Figure 2(b) we compare a quadratic interpolation to $\bar{D}$ with the exact value. It seems that the quadratic interpolation is essentially the same as the exact value; however, since our geometry itself is only a model, even the linear interpolation is very good. A similar interpolation can also be shown for other local geometries, such as the one depicted in Figure 1(b).

Example 1: Our first test is carried out for the reaction diffusion alone, neglecting the effect of changes in the enamel geometry. This is certainly justified for short time periods, following the estimate we gave in the previous section on the dissolution rate for pH value of about 4. The cell consists of a single disc of radius ρ. Symmetry implies that in this case the effective diffusion tensor $\bar{D}$ is diagonal, and therefore the suppression of the x_2 variable does not have a serious effect on the problem. For this geometry we computed the effective horizontal diffusion coefficient for $\rho = 0.9$ and found $\bar{D} = 0.72$.

We solve for the specific scenario where the system is at equilibrium, and then is disturbed by a burst of acidity (low pH) for a certain time period. To fix ideas, we assume that $H = 10^{-5}$ at all the boundaries

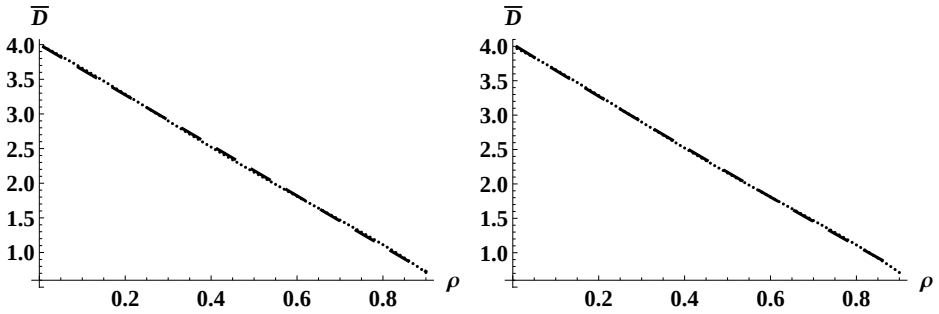

Figure 2. The effective diffusion coefficient $\bar{D}(\rho)$ for the geometry of Figure 1(a) as a function of the local geometry (dotted line) compared with approximations of it (dashed lines). (a) Linear interpolation $\bar{D}(\rho) = 4 - 3.64\rho$, (b) Quadratic interpolation $\bar{D}(\rho) = 4.03 - 3.82\rho + 0.2\rho^2$.

except at the top of the tooth ($x_3 = 0$ in our convention). For the time period, $0 < t < T = 72$ we simulate the burst of low pH by setting the boundary condition $H(x_1, 0; t) = 10^{-5} + 9 \cdot 10^{-5} A(0.1 - |x_1|)$, where $A(\xi)$ is the Heaviside function.

Given H, and neglecting the change in Ω and $|\partial E_p|$ we solve equation (5.9). We set the boundary condition $q = 10^{-5}$ over the entire boundary. While this is a reasonable condition on the lateral boundaries, and also deep inside the tooth, it is not so obvious at the tooth edge $x_3 = 0$. However, we point out that this condition stabilizes q in the sense that it acts to inhibit demineralization. This is consistent with the physiology of the tooth, where there is an external thin layer near the surface that is resilient to demineralization. The initial condition is set to be $q \equiv 10^{-5}$.

Because of the similarity of the equations and boundary conditions for H and q, we can simplify the calculations by defining the difference function $v(x,t) = H - q$. Thus, v solves

$$(|\Omega| v)_t = \left(|\Omega| v_{x_3}\right)_{x_3} + \sum_{i=1}^{2} \partial_{x_i} \left(\bar{D}_{ij} \partial_{x_j}\right) v - |\partial E_p| R_1 v, \tag{6.1}$$

with the appropriate boundary conditions set above.

Upon solving for q and H (or for v), we can compute the evolution of $\rho(x,t)$ according to equation (5.10). Recall that in this example, while we compute $\rho(x,t)$ we do not change the geometry. Since the change in ρ is small in this time interval, we express ρ in the form $\rho = \rho_0 + 10^{-4}\rho_1(x,t)$, where ρ_0 is the original (constant) value of ρ. Therefore $\rho_1(x,t)$ solves the equation

$$\partial_t \rho_1 = -\frac{10^4 R_1}{6} \gamma (H - q) = -\frac{10^4 R_1}{6} \gamma v, \tag{6.2}$$

where $R_1 = 1$.

The progression of caries, as calculated in this example, is presented in Figure 3. In Figure 3(a) we draw the tip of the level set $\rho_1 = -15$ as a function of t. In Figure 3(b) we draw the same level set tip, but now as a function of $t^{1/2}$. In Figure 3(c) we depict the total enamel volume $\tilde{E}$ as a function of t. We chose these specific graphs in order to compare our model, at least quantitatively, with well-known experiments. There is a debate in the literature as to what is the actual rate of caries progression.

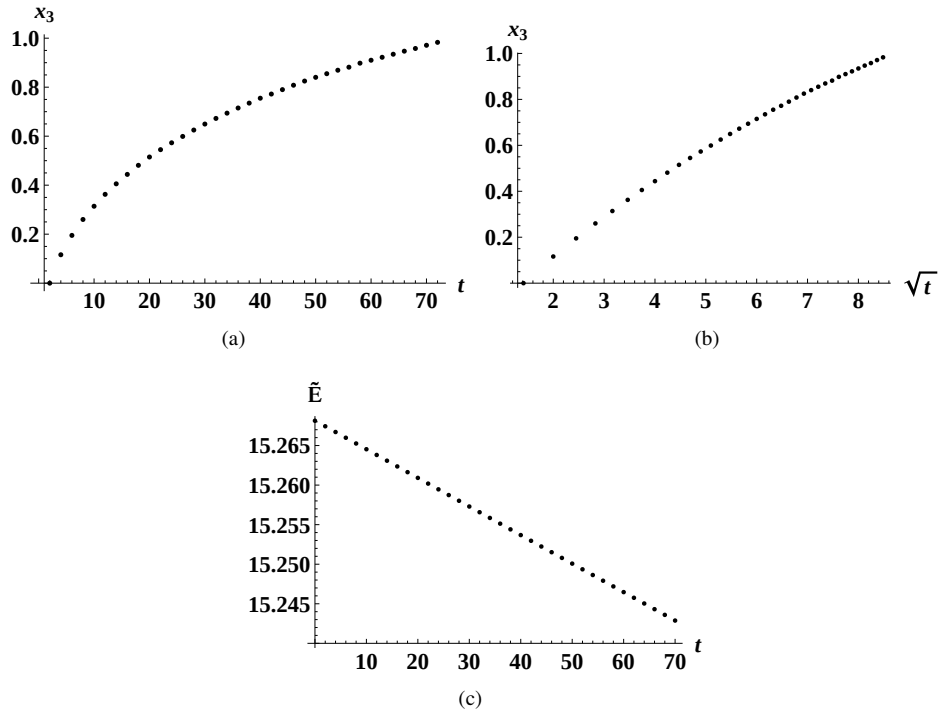

Figure 3. Progression of caries for the first boundary condition of Example 1: (a) Motion of x_3, the tip of a level set of ρ_1, (b) Motion of the same level set as a function of $t^{1/2}$, (c) The evolution of the total enamel volume $\tilde{E}(t)$

Anderson et al. Anderson *et al.* (1998) cite a number of authors that argue that caries progresses as a linear function of $t^{1/2}$. A typical result along this line is the paper of Poole et al. Poole & Shellis *et al.* (1981). On the other hand, many authors, and in particular Anderson himself, provide experimental evidence that caries progresses linearly in t.

We argue that the progression rate depends on how one defines it. This can be seen from the present example. When the total enamel volume lost to reaction is computed, which corresponds to the decline in $\tilde{E}$ in our case, the progression is linear. This follows directly from our equations. Consider first the evolution of ρ (5.10). The evolution of $|\tilde{E}|_t$ is proportional to the integral of $\rho\rho_t$. From equation (5.10) this, in turn, is proportional to the integral of ρv. Since the evolution of v, which is determined by equation (6.1), stabilizes in a few hours, the integral of ρv is proportional to the total flux of v (a conclusion that is simply the law of mass conservation). However, since the evolution of ρ is slow on the relevant time scale, the flux is approximately constant in time, and therefore the evolution of $\tilde{E}$ is linear in time. This argument is indeed manifested in Figure 3(c).

A number of authors, including for example Poole & Shellis *et al.* (1981) and Featherstone (1977), claim that the progression of caries is proportional to $t^{1/2}$. The theoretical justification, see for example Van Duk & Borggreven *et al.* (1983), is that for a short time period caries is dominated by diffusion, and at least initially, and in a one-dimensional approximation, the concentration of the ions is proportional to $\mathrm{Erf}(x_3/2(Dt)^{1/2})$. However, with the observed value of the diffusion coefficient D, and the typical scaling for caries, this description is only valid for a couple of hours at most. Therefore it cannot be used

for experiments like those in reference Poole & Shellis *et al.* (1981), for example, where the enamel was exposed to large acidity for days.

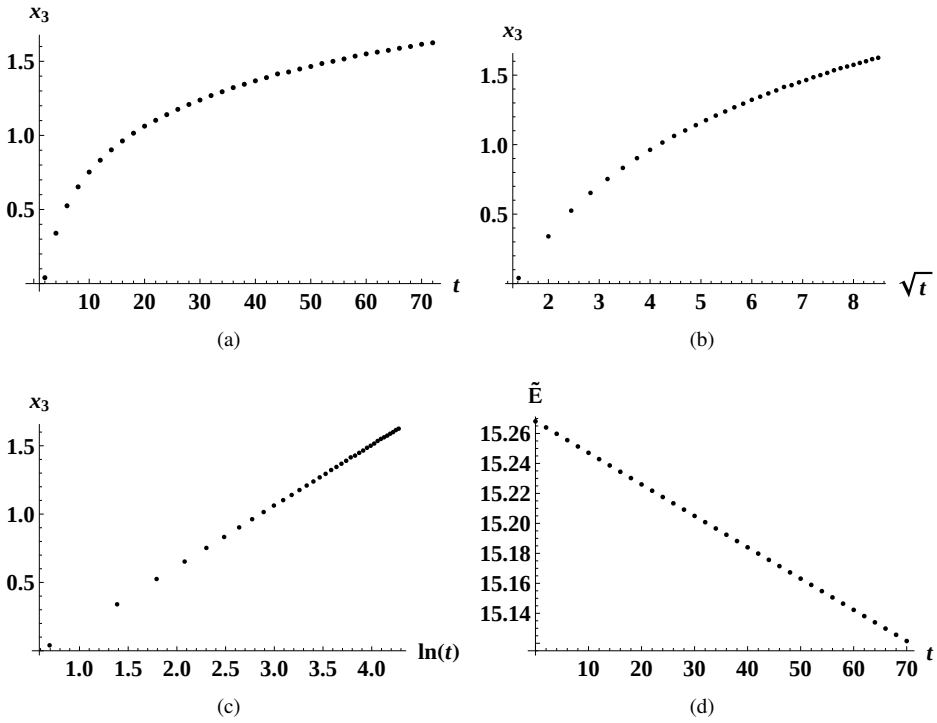

Figure 4. Progression of caries for the boundary condition $v(x_1,0,t) = 10^{-4}\cos(\pi x_1/2)$: (a) Motion of x_3, the tip of a level set of ρ_1, (b) Motion of the same level set as a function of $t^{1/2}$, (c) Motion of the same level set as a function of $\ln t$, (d) The evolution of the total enamel volume $\tilde{E}(t)$.

The authors in references Poole & Shellis *et al.* (1981) and Featherstone (1977) (and similar publications) visually inspected the lesion, and deduced the progression from this inspection. This is similar to following the tip of a specific value of ρ, as depicted in Figure 3(a). It is tempting to associate this curve with some power law. For instance, we drew in Figure 3(b) the motion of the level set as a function of $t^{1/2}$. This curve looks approximately linear. However, selecting a power law can be misleading. We draw attention to the recent analysis of Stumpf and Porter Stumpf & Porter (2012). They showed that power law expressions empirical studies is often unjustified. To demonstrate this point in the present context, we performed another numerical test, where we replaced the boundary condition above for H and q by the boundary condition (for their difference) $v(x_1,0,t) = 10^{-4}\cos(\pi x_1/2)$.

The advantage of selecting this boundary condition is that after a short time period the function v reaches a steady state that can be solved explicitly. For the specific parameters in this example we have that in the steady state v solves $v_{x_3x_3} + 1/2v_{x_1x_1} - 3.87v = 0$. Thus, approximately we have

$$v \sim 10^{-4}\cos(\pi x_1/2)e^{-2.25x_3}.$$

The equation for ρ then implies that level sets of ρ evolve (for $t > 1$, say) approximately according to

$$x_3(t) = 0.44 \ln t + C, \tag{6.3}$$

for some constant C. Indeed the computed curve of $x_3(t)$ is shown in Figure 4(a), and the linear dependency of x_3 on $\ln t$ is clearly observed in Figure 4(c), with the predicted slope.

Example 2: We compare here two simulations. We use the same geometry as in Example 1, with boundary condition $q = 10^{-5}$ over the entire boundary and initial condition $q \equiv 10^{-5}$. Also, we assume that $H = 10^{-5}$ at all the boundaries except at the top of the tooth, but. We solve for the time period, $0 < t < T = 264$ (11 days), and the boundary conditions at $x_3 = 0$ are given by $H(x_1, 0; t) = 10^{-5} + 5 \cdot 10^{-4} A(0.1 - |x|)$, which simulates relatively low pH.

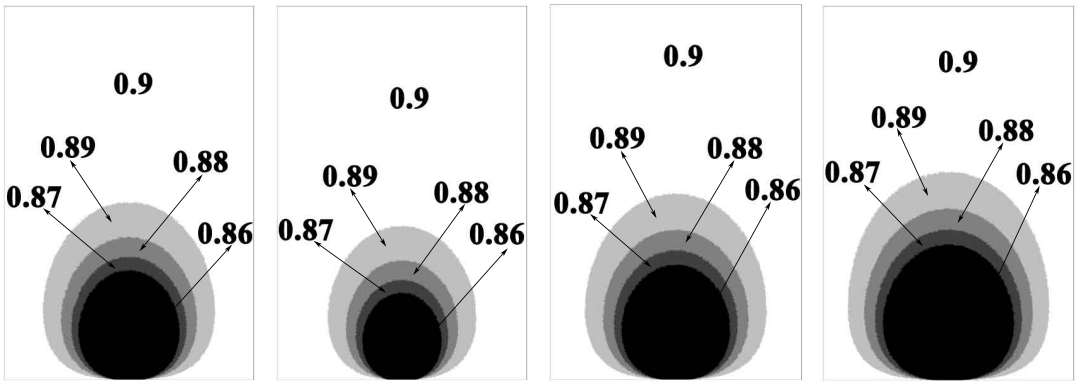

(a) $t = 264$ (b) $t = 120$ (c) $t = 192$ (d) $t = 264$

Figure 5. (a) Level sets of $\rho(x, t = 264)$ for the boundary conditions of Example 2, neglecting the evolution of the geometry and of $\bar{D}$. (b)-(d) Level sets of $\rho(x,t)$ for three values of t for the boundary conditions of Example 2. Here the evolution of the geometry and of $\bar{D}$ was taken into account.

In the first simulation (Figure 5(a)) we fixed the geometry, i.e. ρ at its initial value $\rho = 0.9$. we compute $\rho(x,t)$ as in Example 1 above, and draw the level sets of $\rho(x, 264)$. In the second simulation we update $\rho(x,t)$ throughout the evolution of v. We draw for comparison the level set at $\rho(x, 120)$, (Figure 5(b)), $\rho(x, 192)$ (Figure 5(c)), and $\rho(x, 264)$ (Figure 5(d)). Since the enamel melts appreciably in this long time interval, ρ decreases and thus $\bar{D}$, which is now a function of space and time increases. As a results, we see a faster progression of caries in Figure 5(d) than in Figure 5(a).

7. Discussion

We presented a model for the progression of dental caries lesions. We start from a model for the microscopic geometry. The local reaction diffusion equations are homogenized, while taking into account the change of the geometry in space and time because of the dissolution of the enamel. The global macroscopic equations include important features such as anisotropic diffusion, resulting from the local geometry, an effective reaction term, and an equation for the evolution of the geometry. The equations are nonlinear due to the mutual coupling of the reaction-diffusion and the geometry.

To demonstrate the effective equations we considered the progression of caries in a rectangular domain. We chose this geometry for its simplicity and because it is essentially the geometry used in many experiments. In our examples we concentrated on two issues. One is the effect of the anisotropy and of the melting. This is best seen in Example 2 in the preceding section. Caries is seen to propagate faster along the "easy" x_3 axis, than in the orthogonal direction. The effect of dissolution is observed by comparing Figure 5(a) to Figure 5(d). In both cases the equations were solved for a long period of time under conditions of low pH. However, in the first case we neglected the change in the geometry, and in the second case we updated the geometry, and also the diffusion coefficient. Indeed in the second case caries propagated faster also in the horizontal direction.

Another goal of our numerical simulation was to consider the question of progression rate of caries. A number of conflicting theories appear in the literature. We demonstrated in the preceding section that the progression rate depends on the way it is defined. We also pointed out that some of the power laws proposed in the literature are questionable.

The preliminary model presented here can be extended in a number of ways. First, the model can be embedded in a realistic tooth geometry. This will enable to study the effect of the tooth surface on caries progression. Another extension, that we already pointed out in the introduction is to consider separate reaction diffusion equation for the different compounds in the reaction. A third extension is to build into the model the hard external layer near the tooth surface that is more resilient to caries. Furthermore, adding compounds such as fluoride to the model will enable applying the model to study medical treatments for arresting caries. We are indeed working on upgrading our model in these directions.

8. Appendix: Proof of some geometric formula

We prove in this appendix some of the geometric formula we used earlier in deriving the averaged equation of the concentration c.

To prove formula (3.4) for the normal $\hat{n}$ we write

$$\hat{n} = \alpha \left(F_{y_1} + \varepsilon F_{x_1}, F_{y_2} + \varepsilon F_{x_2}, \varepsilon F_{x_3} \right),$$

where α is a factor chosen so $\hat{n}$ has unit norm. To leading order we obtain

$$\alpha = 1/G_F \left(1 - \varepsilon \nabla_2^y F \cdot \nabla_2^x F / G_F^2 \right).$$

Therefore

$$\hat{n} = \hat{\nu} + \varepsilon / G_F \left(\nabla_2^x F - \hat{\nu} (\hat{\nu} \cdot \nabla_2^x F) + \hat{k} F_{x_3} \right).$$

Formula (3.4) follows from the last identity.

To prove the first formula of (3.25) we observe that the volume of Ω is $|\Omega| = 1 - |E_p|$, can also be written as as

$$|\Omega| = (1 - \int_{cell} \chi_{E_p} \, dy),$$

where χ_{E_p} is the characteristic function of E_p. We then notice the relation $\partial_t \chi_{E_p} = \delta(x - \partial E_p) v_V$. Substituting the last relation into the equation

$$\partial_t |\Omega| = - \int_{cell} \partial_t \chi_{E_p} \, dy \tag{8.1}$$

leads to the first formula of (3.25).

The second identity of equation (3.25) and identity (3.22) follow from the following general argument: Let θ be any of the arguments (x_1, x_2, x_3) of the function F introduced in equation (3.3). To emphasize that we concentrate on this argument we write

$$\partial E_p(\theta) : \{F(y_1, y_2, \theta) = 0\}.$$

We now show that

$$\frac{\partial}{\partial \theta}|E_p| = -\int_{\partial E_p} F_\theta / G_F. \tag{8.2}$$

To find the change in the area of E_p as we vary the parameter θ we need to find the area of ring between $E_p(\theta)$ and $E_p(\theta + d\theta)$. To find the thickness of the ring we move a distance δ along the normal ν. To determine δ we expand the relation $F(y_1 + \delta F_{y_1}/G_F, F_{y_2} + \delta F_{y_2}/G_F, \theta + \delta\theta) = 0$. Using also $F(y_1, y_2, \theta) = 0$ we obtain $\delta = -F_\theta d\theta / G_F$. Therefore $d\delta/d\theta = -F_\theta / G_F$. This proves (8.1)

Acknowledgment

This work is supported in part by a F.I.R.S.T. Initial Training Grant of the ERC, and in part by a grant from the ISF. We thank Dr. Marc Campillo for useful discussion on caries and for bringing a few references to our attention.

References

ANDERSON, P., LEVINKIND, M. & ELLIOTT, J.C. (1998) Scanning microradiographic studies of rates of in vitro demineralization in human and bovine dental enamel, *Arch. Oral Biol.,* **43**, 649–656.

BJORLAND, L. & THYLSTRUP, A. (1995) A strucutral analysis of approximal enamel caries lesions and subjacent dentin reactions, *Eur. J. Oral Sci.,* **103**, 25–31.

BJORLAND, L. (2008) The caries process and its effect on the pulp: The science is changing and so is our understanding, *Pediatric Dentistry,* **30**, Vol 3.

BOLLET-QUIVOGNE, S.E.C., ANDERSON, P., DOWKER, S.E.P. & ELIOTT, J.C., (2005) Microradiographical study on the influence of diffusion in the external liquid on the rate of demineralization in hydroxyapatite aggregates, *Euro. J. Oral Sci.,* **113**, 53–59.

FEATHERSTONE, J.D.B. (1977) *Diffusion phenomena during artificial carious lesion formation. J. Dental Res.,* **56**, D48.

HOLLY, F.J. & GRAY, J.A., (1968) Mechanism for incipient carious lesion growth utilizing a physical model based on diffusion concepts, *Arch. Oral Biol.,* **13**, 319–334.

KIDD, E.A.M. & FEJERSKOV, O. (2004) What constitutes dental caries? Histopathology of carious enamel and dentin related to the action of cariogenic biofilms. *J. Dent. Res.,* C35–C38.

PATEL, M.V., FOX, J.L. & HIGUCHI, W.I. (1987) Physical model of non steady state dissolution of dental enamel, *J. Dental Research,* **66**, 1418–1424.

PATEL, M.V., FOX, J.L. & HIGUCHI, W.I. (1987) Higuchi, Effect of acid type on kinetics and dissolution of dental enamel demineralization, *J. Dental Research,* **66**, 1425–1430.

POOLE, D.F.G., SHELLIS, R.P. & TYLER, J.E., (1981) Rates of formation in vitro of dental caries-like enamel lesion in man and some non-human primates, *Arch. Oral Biol.,* **26**, 413–417.

STUMPF, M.P.H. & PORTER, M.A., (2012) Criticla truths about power laws, *Science,* **335**, 665–666. **6**, 133–152.

VAN DUK, J.W.E., BORGGREVEN, J.M.P.M. & DRIESSENS, F.C.M., (1983) Diffusion in mammalian tooth enamel in relation to the caries process, *Arch. Oral Biol.,* **28**, 391–397.

ZIMMERMAN, S.O., (1966) A mathematical theory of enamel solubility and the onset of dental caries, part III, *Bull. Math. Biophys.,* **28**, 443–464.